Editors' Suggestion

Global description of β^- decay with the axially deformed Skyrme finite-amplitude method: Extension to odd-mass and odd-odd nuclei

E. M. Ney,[1,*] J. Engel,[1,†] T. Li (李通),[2,‡] and N. Schunck[3,§]

[1]*Department of Physics and Astronomy, CB 3255, University of North Carolina, Chapel Hill, North Carolina 27599-3255, USA*

[2]*Department of Physics and Astronomy and National Superconducting Cyclotron Laboratory, Michigan State University, East Lansing, Michigan 48824, USA*

[3]*Nuclear and Chemical Science Division, LLNL, Livermore, California 94551, USA*

(Received 24 May 2020; accepted 26 August 2020; published 28 September 2020)

We use the finite-amplitude method (FAM), an efficient implementation of the quasiparticle random phase approximation, to compute β-decay rates with Skyrme energy-density functionals for 3983 nuclei, essentially all the medium-mass and heavy isotopes on the neutron-rich side of stability. We employ an extension of the FAM that treats odd-mass and odd-odd nuclear ground states in the equal filling approximation. Our rates are in reasonable agreement both with experimental data where available and with rates from other global calculations.

DOI: 10.1103/PhysRevC.102.034326

I. INTRODUCTION

The origin of elements heavier than iron still remains an open question. Early work has shown that neutron capture in astrophysical processes is responsible for synthesizing those elements [1,2]. Rapid neutron capture, through the "*r* process," is particularly interesting because its astrophysical site is still uncertain. The multimessenger neutron star merger GW170817 [3] recently provided evidence that such events are the dominant source of *r*-process elements, but quantitative conclusions require more data. We need more reliable astrophysical simulations to connect future multimessenger events with details of the underlying nucleosynthesis.

Abundances of *r*-process elements depend on a variety of nuclear properties, including masses, neutron-capture cross sections, photodisintegration cross sections, fission yields, and β-decay half-lives [4]. Although some of these properties have been measured and tabulated [5], the majority of nuclei relevant for the *r* process are too unstable to be produced in the laboratory. Reliable *r*-process simulations thus require calculations in neutron-rich nuclei. βeta-decay half-lives are particularly important because they determine the overall time scale for neutron capture in the *r* process [6,7] and affect the shape of the final abundance pattern [8,9].

A variety of global β-decay calculations exist, in the semigross theory [10], in a quasiparticle random-phase approximation (QRPA) plus the macroscopic finite-range droplet model (FRDM) approach [6,11], in covariant density functional theory (DFT) [12], etc. DFT, covariant or not, is particularly attractive because it offers a self-consistent, microscopic framework for computing properties across the nuclear chart [13,14]. For the calculation of β decay in deformed superfluid nuclei, DFT amounts to the QRPA, built on a ground state produced by the Hartree-Fock-Bogoliubov (HFB) method, which incorporates pairing correlations into mean fields, all with density-dependent interactions.

In odd-mass and odd-odd nuclei (hereafter "odd" nuclei) pairing is "blocked" and the HFB ground state contains a quasiparticle excitation [13]. This complicates calculations because the ground state is no longer invariant under time reversal [15,16]. As a result additional approximations are often made in β-decay calculations. Reference [17], for example, treats one-quasiparticle states perturbatively, while Ref. [12] treats them as if they were zero-quasiparticle states. A more consistent way to approximate HFB blocked states while preserving time-reversal symmetry is through the equal filling approximation (EFA) [18]. Numerous studies showed that the EFA is an excellent approximation to exact blocking [16,19,20]. Reference [9] recently developed a method to extend the EFA to the QRPA.

In this work we use the extension to carry out a global calculation of allowed and first-forbidden contributions to β-minus decay in odd nuclei from near the valley of stability out to the neutron drip line. We use a global Skyrme density functional determined in Ref. [21], thus extending that work, which was restricted to even-even nuclei, to all isotopes that play a role in the *r* process.

This rest of this paper is as follows: Sec. II presents background for the finite-amplitude method (FAM), which we use to compute QRPA strength functions, and its extension to the EFA. Section III outlines some improvements to our implementation of the FAM since the work of Ref. [21]. Section IV presents our results, compares them to those of other papers and to experiment, and addresses subtleties of the EFA-FAM. Section V contains concluding remarks.

*evan.ney@unc.edu
†engelj@physics.unc.edu
‡lit@nscl.msu.edu
§schunck1@llnl.gov

II. THE PROTON-NEUTRON FINITE-AMPLITUDE METHOD (PNFAM)

A. The pnFAM for pure states

The QRPA linear-response function is the same as that from time-dependent HFB theory [13]. One way of computing is to diagonalize a set of matrices with dimension equal to that of the two-quasiparticle space. The construction of these matrices, which require two-body matrix elements of the potential, is time consuming in deformed nuclei. The FAM sidesteps the matrices, significantly speeding up the computation of linear response produced by energy-density functionals. Reference [22] first presented the FAM for the ordinary RPA, and Ref. [23] did the same for the QRPA. Since then, the method was used with covariant density functionals [24–26] and employed to compute transition strength in several contexts [27–31].

Here we build on the work of Refs. [9,21,32], which used a charge-changing version of the FAM called the pnFAM together with the contour-integral method of Refs. [33–36] to compute β-decay rates. A detailed account of the pnFAM and its application to β decay appears in Ref. [32]. Reference [9] used the EFA to extend the pnFAM to odd nuclei and compute β-decay rates in the rare-earth nuclei that are important for r-process simulations. To highlight a few subtleties of the EFA-pnFAM, we recapitulate the main points of the theory here.

We begin with the time-dependent HFB equations,

$$i\dot{\mathbb{R}}(t) = [\mathbb{H}[\mathbb{R}(t)] + \mathbb{F}(t),\ \mathbb{R}(t)]. \tag{1}$$

Here, $\mathbb{R}$ is the generalized HFB density matrix, $\mathbb{H}$ is the HFB Hamiltonian matrix, and $\mathbb{F}$ is a matrix that represents a one-body time-dependent perturbation. The blackboard-bold letters indicate that these matrices are in the HFB quasiparticle basis, defined by the Bogoliubov transformation $\mathbb{W}$:

$$\mathbb{W} = \begin{pmatrix} U & V^* \\ V & U^* \end{pmatrix}, \tag{2}$$

where U and V are themselves matrices. In this basis the static ground-state Hamiltonian and the associated generalized density are diagonal:

$$\mathbb{H}_0 = \begin{pmatrix} E & 0 \\ 0 & -E \end{pmatrix}, \quad \mathbb{R}_0 = \begin{pmatrix} 0 & 0 \\ 0 & 1 \end{pmatrix}. \tag{3}$$

To first order in the perturbation $\mathbb{F}$, Eq. (1) is

$$i\delta\dot{\mathbb{R}}(t) = [\mathbb{H}_0, \delta\mathbb{R}(t)] + [\delta\mathbb{H}(t) + \mathbb{F}(t), \mathbb{R}_0], \tag{4}$$

with $\delta\mathbb{R}(t) = \mathbb{R}(t) - \mathbb{R}_0$. If the perturbation is harmonic, the time-dependent quantities $\mathbb{F}(t)$, $\delta\mathbb{H}(t)$, and $\delta\mathbb{R}(t)$ all take the form (e.g., for $\mathbb{F}$),

$$\mathbb{F}(t) = \mathbb{F}(\omega)e^{-i\omega t} + \mathbb{F}^\dagger(\omega)e^{i\omega t},$$
$$\mathbb{F}(\omega) = \begin{pmatrix} F^{11}(\omega) & F^{02}(\omega) \\ -F^{20}(\omega) & -F^{\overline{11}}(\omega) \end{pmatrix}. \tag{5}$$

We denote the perturbed density more specifically by

$$\delta\mathbb{R}(\omega) = \begin{pmatrix} P(\omega) & X(\omega) \\ -Y(\omega) & -Q(\omega) \end{pmatrix}. \tag{6}$$

When one substitutes Eqs. (5) and (6) into Eq. (4), the diagonal blocks P and Q vanish, and for a charge-changing external field only the proton-neutron matrix elements of the response are nonzero. These conditions lead to the pnFAM equations,

$$\begin{aligned}(E_\pi + E_\nu - \omega)X_{\pi\nu}(\omega) &= -\big(\delta H^{20}_{\pi\nu}(\omega) + F^{20}_{\pi\nu}(\omega)\big),\\ (E_\pi + E_\nu + \omega)\,Y_{\pi\nu}(\omega) &= -\big(\delta H^{02}_{\pi\nu}(\omega) + F^{02}_{\pi\nu}(\omega)\big),\end{aligned} \tag{7}$$

where the label π denotes protons and the label ν denotes neutrons. The use of a finite-difference method to compute δH is the source of the FAM's speed. Because we do not consider mixing of protons and neutrons in the underlying HFB ground state, and because Skyrme functionals in use depend at most quadratically on charge-changing densities, the finite difference in the pnFAM reduces exactly to the evaluation of the Hamiltonian with the perturbed densities:

$$\begin{aligned}\delta\mathbb{H}^{(pn)} &= \lim_{\eta\to 0}\frac{1}{\eta}\Big(\mathbb{H}\big[\mathbb{R}_0^{(pp,nn)} + \eta\delta\mathbb{R}^{(pn)}\big] - \mathbb{H}\big[\mathbb{R}_0^{(pp,nn)}\big]\Big)\\ &= \mathbb{H}[\delta\mathbb{R}^{(pn)}].\end{aligned} \tag{8}$$

Once the FAM amplitudes X and Y are known, one can compute the strength function:

$$\frac{dB(F,\omega)}{d\omega} = -\frac{1}{\pi}\mathrm{Im}S(F,\omega), \tag{9}$$

where

$$\begin{aligned}S(F,\omega) &= \sum_{\pi\nu}\big[F^{20^*}_{\pi\nu}X_{\pi\nu}(\omega) + F^{02^*}_{\pi\nu}Y_{\pi\nu}(\omega)\big]\\ &= -\sum_n\left(\frac{|\langle n|\hat{F}|0\rangle|^2}{\Omega_n - \omega} + \frac{|\langle n|\hat{F}^\dagger|0\rangle|^2}{\Omega_n + \omega}\right).\end{aligned} \tag{10}$$

The FAM strength function has poles at QRPA excitation energies Ω_n with residues equal to the transition probabilities $|\langle n|\hat{F}|0\rangle|^2$. It also contains poles at $-\Omega_n$, with residues equal to the negative of transition probabilities for the conjugate operator $|\langle n|\hat{F}^\dagger|0\rangle|^2$. In β-minus-decay calculations $\hat{F}$ contains the isospin lowering operator and $\hat{F}^\dagger$ contains the isospin raising operator; cf. Ref. [32] for a list of the six allowed and first-forbidden operators. Thus, the poles with positive and negative residues correspond to β-minus and β-plus transitions, respectively. This point will become important in the EFA-pnFAM.

In practice we construct the strength function by solving the pnFAM equations separately for each of a large set of complex frequencies ω. From Eqs. (9) and (10), it is straightforward to show that each pole of $S(F,\omega)$ on the real axis contributes a Lorentzian of half-width $\gamma = \mathrm{Im}[\omega]$ to the strength function in the complex plane. The strength may be calculated for a set of frequencies close to the real axis with a fixed half-width to mimic experimental strength measurements, or along a closed contour in the complex plane to calculate cumulative strength or decay rates.

B. The pnFAM for statistical ensembles

Many HFB codes use the EFA to avoid the difficulties associated with the breaking of time-reversal symmetry [13,15] in odd nuclei. The originally *ad hoc* EFA can be understood as

a special case of statistical HFB theory for an ensemble that is symmetric under time reversal [16,18]. In systems with time-reversal symmetry, a state $|\lambda\rangle$ and its time-reversed partner $|\bar{\lambda}\rangle$ are degenerate, and the equal filling quasiparticle occupation probabilities, for axial but not spherical symmetry, are

$$f_{\mu\nu} = \tfrac{1}{2}(\delta_{\nu\lambda} + \delta_{\nu\bar{\lambda}})\delta_{\mu\nu}. \tag{11}$$

In odd-odd nuclei, both the odd-proton and odd-neutron quasiparticles have nonzero occupation probabilities. Note that in this work, we do not consider neutron-proton pairing at the HFB level.

The statistical extension of the QRPA [37] lets us use the FAM to treat excitations of HFB ensembles, taking into account at least partially the polarization of the even-even "core" by the odd nucleon. The EFA-FAM can be derived in the same way as the ordinary FAM, by promoting the ground-state generalized density matrix to a statistical density operator. Expectation values that, for example, define the particle densities, then become ensemble averages. The generalized HFB density matrix is no longer a projector and takes the more general form,

$$\widetilde{\mathbb{R}}_0 = \begin{pmatrix} f & 0 \\ 0 & 1-f \end{pmatrix}. \tag{12}$$

In the usual finite-temperature theory, based on the grand canonical ensemble, the occupation probabilities are given by $f_{\mu\nu} = (1 + \exp(\beta E_\mu))^{-1}\delta_{\mu\nu}$ [38]. In the EFA we impose the occupation probabilities of Eq. (11).

To obtain the statistical pnFAM equations we simply replace the ground-state generalized density of Sec. II A with that of Eq. (12). The diagonal elements of the density response no longer vanish, and new statistical factors appear. Once again, for a charge-changing perturbation we need only the proton-neutron matrix elements, and so the statistical pnFAM equations are

$$\begin{aligned}
(E_\pi - E_\nu - \omega)P_{\pi\nu}(\omega) &= -(f_\nu - f_\pi)(\delta H + F)^{11}_{\pi\nu}(\omega), \\
(E_\pi + E_\nu - \omega)X_{\pi\nu}(\omega) &= -(1 - f_\pi - f_\nu)(\delta H + F)^{20}_{\pi\nu}(\omega), \\
(E_\pi + E_\nu + \omega)Y_{\pi\nu}(\omega) &= -(1 - f_\pi - f_\nu)(\delta H + F)^{02}_{\pi\nu}(\omega), \\
(E_\pi - E_\nu + \omega)Q_{\pi\nu}(\omega) &= -(f_\nu - f_\pi)(\delta H + F)^{\overline{11}}_{\pi\nu}(\omega).
\end{aligned} \tag{13}$$

The additional P and Q amplitudes arise because the nonzero occupation probabilities allow quasiparticles to be destroyed as well as created. The new transitions introduce an additional set of QRPA eigenvalues that contain quasiparticle-energy differences rather than sums [37]. It is possible for these energy differences to be negative, indicating a transition to a state of lower energy. This does not mean, however, that the QRPA fails, as it does when the eigenvalues are imaginary. The statistical FAM strength has the same form as the usual strength in Eq. (10), but the residues become ensemble-averaged transition strengths, and n runs over the expanded set of QRPA modes. More details on the EFA-FAM and a demonstration that it includes all necessary transitions for odd states, in the context of the particle-rotor model [39], appear in Ref. [9].

III. COMPUTATIONAL METHOD

A. HFB ground states and functional

In obtaining our global set of half-lives, we introduce a number of small improvements to the procedure of Ref. [21], in addition to the changes required to compute half-lives of odd nuclei. The first is in the determination of the HFB ground state/ensemble. To make sure that we identify the correct ground state, we perform three different calculations for each even-even nucleus by constraining the first 10 iterations of the HFB solver to an oblate, spherical, and prolate quadrupole shape before releasing the constraint. In contrast to Ref. [21], which used a set of three fixed quadrupole constraints for all nuclei, we use the first-order mass-dependent relation [13],

$$Q_2 = \frac{5}{100\pi}\beta_2 A^{5/3}, \tag{14}$$

with values $\beta_2 = -0.2, 0.0, +0.2$. This procedure gives one, two, or three different deformed minima, depending on the even-even nucleus. We then identify a number of candidate quasiparticle states within 1 MeV of the Fermi surface to block in the EFA. For odd-odd nuclei we consider all possible combinations of proton and neutron candidates. For every candidate (or candidate pair), we carry out the EFA on top of each available deformed even-even core, without constraints, and select the solution with the lowest energy. On occasion these are metastable superdeformed states, which we discard.

We use the Skyrme functional SKO′ [40], which was found in Ref. [21] to give accurate Q values across the nuclear chart. We fit the like-particle pairing strengths to the experimental pairing gaps of 10 isotopes picked in a wide mass range $50 \leqslant A \leqslant 230$, and apply an ultraviolet cutoff of 60 MeV to the single-particle space. For the pnFAM portion of the calculation we set the time-odd parameters and isoscalar pairing strength to the values determined in the fit "1A" of that reference. We therefore also use the same 16-shell deformed harmonic-oscillator basis that was used in the original fit. All HFB calculations are performed with the latest version of the HFBTHO code [41].

Figure 1 shows the differences between computed Q values—obtained from the HFB calculation in the initial nucleus, Eq. (16), and the approximate expression for the lowest QRPA energy in Eq. (18)—and their experimental counterparts. The parameters of SKO′ were determined by fits in even-even nuclei, so it is perhaps unsurprising that the Q values in such nuclei are better predicted than those in odd systems.

B. β-decay half-lives

The next set of changes concerns the computation of the β-decay half-lives, which is discussed in detail in Ref. [32]. The procedure therein allows us to sum the phase-space-weighted strengths to all energetically allowed daughter states. For allowed transitions, we obtain the rate and half-life via

$$\lambda = \frac{\ln 2}{\kappa}\sum_n f(W_n)|\langle n|F|0\rangle|^2, \quad t_{1/2} = \frac{\ln 2}{\lambda}, \tag{15}$$

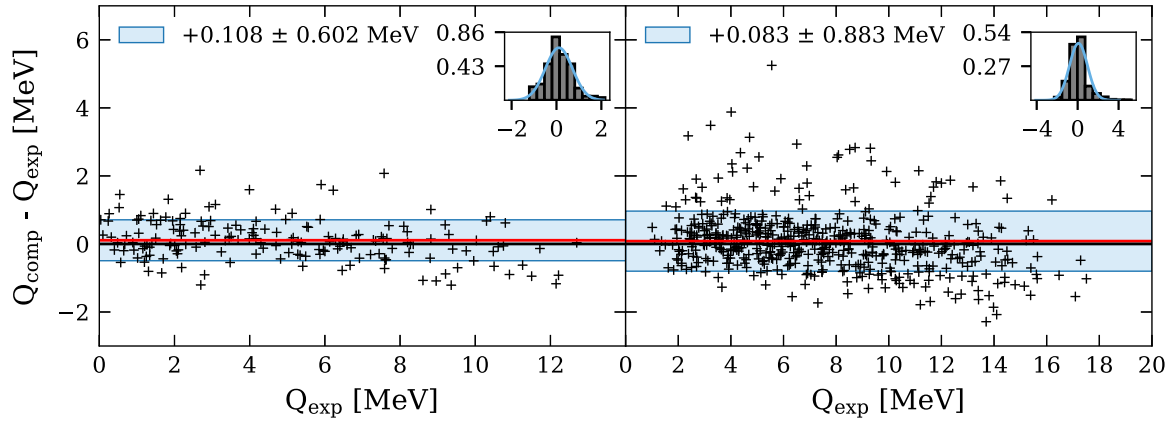

FIG. 1. Differences between computed and experimental Q values for even-even (a) and odd (b) nuclei. The red line is the average difference and the blue band shows one standard deviation, the values of which are given in the legend. The inset shows the normalized histogram of differences under a normal distribution with the same mean and standard deviation as the data.

where $|n\rangle$ is the n^{th} state in the daughter nucleus, $W_n = E_n/m_e c^2$ is the energy, in units of electron mass, of the electron emitted during a transition to that state, and $\kappa = 6147.0 \pm 2.4s$. To include first-forbidden transitions, we must consider a more complicated phase-space-weighted "shape factor" [32]. We evaluate the right side of the first relation in Eq. (15) by integrating the phase-space-weighted strength [Eq. (10)] along a circular complex energy contour [32] that encloses all the poles below the decay Q value. Because the phase-space integral $f(W_n)$ is not analytic, the authors of Ref. [32] fit a polynomial to the integrals on the real axis, and analytically continued the polynomial. High-degree polynomials on evenly spaced grids, however, exhibit the Runge phenomenon [42], and can oscillate rapidly in the complex plane. We therefore elect here to use a rational function to interpolate the phase-space integrals on a 20-point Chebychev grid. Because the contour integrand is quite smooth, we use Gauss-Legendre quadrature to perform the contour integration.

The maximum QRPA energy relevant for β decay defines the right bound of the circular energy contour. With the treatment of Q values in Refs. [7,9,32], the energy released in the transition to the n^{th} state in the daughter nucleus is

$$Q_\beta^{(n)} = \Delta M_{n-H} + \lambda_n - \lambda_p - \Omega_n, \tag{16}$$

where ΔM_{n-H} is the neutron-hydrogen mass difference, λ_p and λ_n are the proton and neutron HFB Fermi energies, and Ω_n ($n \geqslant 1$) is the excitation energy of the n^{th} QRPA mode above the initial-nucleus ground state, after adjustment by the Fermi energies for the change in particle number. (Note that Ω_1 is the "excitation energy" of the ground state of the daughter nucleus.) The maximum QRPA energy, which corresponds to an energy release of zero is then the excitation energy of, e.g., the daughter ground state plus the energy released in the transition to that state,

$$E_{\text{max}}^{\text{QRPA}} = Q_\beta^{(1)} + \Omega_1 = \Delta M_{n-H} + \lambda_n - \lambda_p. \tag{17}$$

and can be evaluated without knowing the daughter ground-state energy itself.

The left bound of the circular energy contour must still be chosen. It must be less than Ω_1, which we do not know exactly, to include all relevant poles in the response. For even-even parent nuclei we can always choose it to be zero because pairing correlations always make Ω_1 positive. For odd parent nuclei, however, Ω_1 can be negative. If we neglect the effects of the QRPA residual interaction, we find explicitly that

$$\begin{aligned}
\Omega_1^{\text{even}} &\approx E_\pi^{\text{smallest}} + E_\nu^{\text{smallest}}, \\
\Omega_1^{\text{n-odd}} &\approx E_\pi^{\text{smallest}} - E_\nu^{\text{blocked}}, \\
\Omega_1^{\text{p-odd}} &\approx E_\nu^{\text{smallest}} - E_\pi^{\text{blocked}}, \\
\Omega_1^{\text{odd-odd}} &\approx -E_\pi^{\text{blocked}} - E_\nu^{\text{blocked}}.
\end{aligned} \tag{18}$$

The fact that Ω_1 can be negative makes it difficult to choose the left bound. If we expand the contour arbitrarily, we risk including β-plus poles with non-negligible negative strength,[1] but if we do not expand it enough, the QRPA residual interaction places Ω_1 outside the contour. Because the pnFAM produces the strength function in Eq. (9) directly, we do not have access to the underlying QRPA eigenvectors and therefore cannot separate β-minus poles from β-plus poles. Both the inclusion of β-plus poles or the accidental exclusion of β-minus poles at negative energies can cause the contour integration to artificially reduce the integrated (and phase-space-weighted) β-minus strength, and therefore artificially increase the half-lives. For lack of a better prescription, we initially choose the left bound of the contour to be

$$E_{\text{min}}^{\text{QRPA}} = \min[0, \Omega_1], \tag{19}$$

with Ω_1 given by the approximations in Eq. (18), but correct the rates as described below when the contour integration appears to lead to errors.

[1]Poles are symmetric around zero, so as soon as β-minus strength appears at negative energy, some β-plus strength (inverted in sign) appears at positive energy.

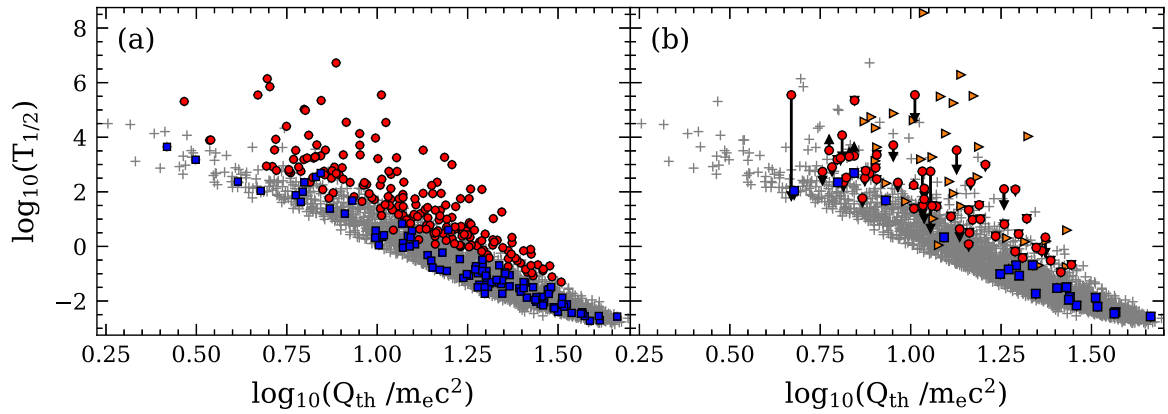

FIG. 2. Corrections of half-lives in odd nuclei. Half-lives for which we calculate strength functions are in (a). Red circles are for the 224 suspicious nuclei and blue squares for the 100 nuclei from the random sample. (b) Half-lives that are corrected as described in the main text, with corrected values indicated by black arrowheads. Orange triangles are corrected versions of originally negative half-lives.

IV. RESULTS

A. Half-lives and odd-nucleus subtleties

To carry out our calculations we bundle the HFB code HFBTHO and the charge-changing FAM code PNFAM together with a controlling python code called PyNFAM. We have improved PNFAM by using matrix multiplication with BLAS rather than explicit loops to construct $\delta\mathbb{H}^{(pn)}$ in the oscillator basis, a step that speeds up execution by a factor of about 10. We calculate the β-minus decay half-lives of nuclei on the neutron-rich side of stability, from $Z = 20$ to $Z = 110$, out to the one-neutron drip line. The lightest nuclei in each isotopic chain are near $A = 50$, and coincide with those used in the global even-even calculation of Ref. [21]. We obtain 3983 ground states, 2998 of which are odd isotopes. Reference [21], which included results to the two-neutron drip line, obtained 1387 even-even ground states with the same functional, versus our 985. Our computation consumed roughly 270 000 Xeon core hours.

Our results in even-even nuclei agree very closely with those of Ref. [21], with a few improvements that can be attributed to our updated procedures. As mentioned in Sec. III B, however, our contour-integration result may be inaccurate in odd nuclei if Ω_1 is less than zero. To assess the validity of the contour integration, we calculate strength functions near the real axis. Though this is a more time-consuming calculation, it allows us to locate β-minus and β-plus poles, determine if there are errors in the contour integration, and decide how to correct incorrect half-lives.

We identify two subsets of nuclei, shown in Fig. 2(a), for which we perform this additional calculation. The first, indicated by red circles, is a set of 224 odd nuclei that have decay rates significantly below the average for a given Q value or that contain significant negative contributions. We refer to this set as "suspicious." The second, shown with blue squares, is a random sample of 100 odd nuclei from the remaining population. Assuming that the probability of a half-life requiring correction is uniformly distributed, this sample size allows us to estimate the proportion of half-lives that require correction with a 10% margin of error at a 95% confidence level. We find that more than half of the examined lifetimes turn out to be correct, and those that are not contain errors of two types.

The first type, illustrated by the top panels of Fig. 3, can be corrected by simply shifting the left bound of the contour. In the figure, the original left bound [Eq. (19)] is the dashed vertical line, while the corrected left bound is the solid vertical line. There are two situations which cause this type of error. The first, similar to that shown in Fig. 3(b), occurs when the HFB estimate Ω_1 is negative but the residual interaction moves it to a positive number $E < |\Omega_1|$. This is corrected by placing the left bound at zero. The second, illustrated in Figs. 3(a) and 3(b), occurs when there exists a β-minus (β-plus) transition at negative (positive) energy, but either the corresponding β-minus or β-plus strength itself is negligible. This behavior occurs almost exclusively in odd nuclei adjacent to closed shells, where pairing vanishes and the transition that takes the parent farther from the closed shell is suppressed. These cases are corrected by shifting the contour to exclude (include) β-minus (β-plus) poles with negligible strength.

The second type of error, exemplified by Fig. 3(c), is more difficult to correct. Two situations can give rise to this shape in the strength distribution: the existence of a non-negligible β-minus pole at negative energy and an associated non-negligible β-plus pole at positive energy, or, as in Figs. 3(c) and 3(d), the existence of poles at imaginary energies. To determine if any corrections are warranted, we pinpoint the location of the poles by calculating the strength parallel to the imaginary axis out to 1 MeV. We examine the strength in each multipole, and if the original contour integration contains any errors, we integrate along a contour that surrounds only the problematic poles (and only them) to determine the correction.

We identify 60 nuclei—54 in the suspicious set and six in the random sample—that require only a simple adjustment of the contour, and 41 nuclei—26 in the suspicious set and 15 in the random sample—that require more careful corrections (33 of which have an imaginary pole in at least one multipole). The results of correcting the half-lives appear in Fig. 2(b). The amount of change is indicated by the black arrowheads. Most of the arrowheads lie hidden beneath the circles or squares, usually because the problems are in forbidden multipoles that contribute only a small amount to the rate. Only a few

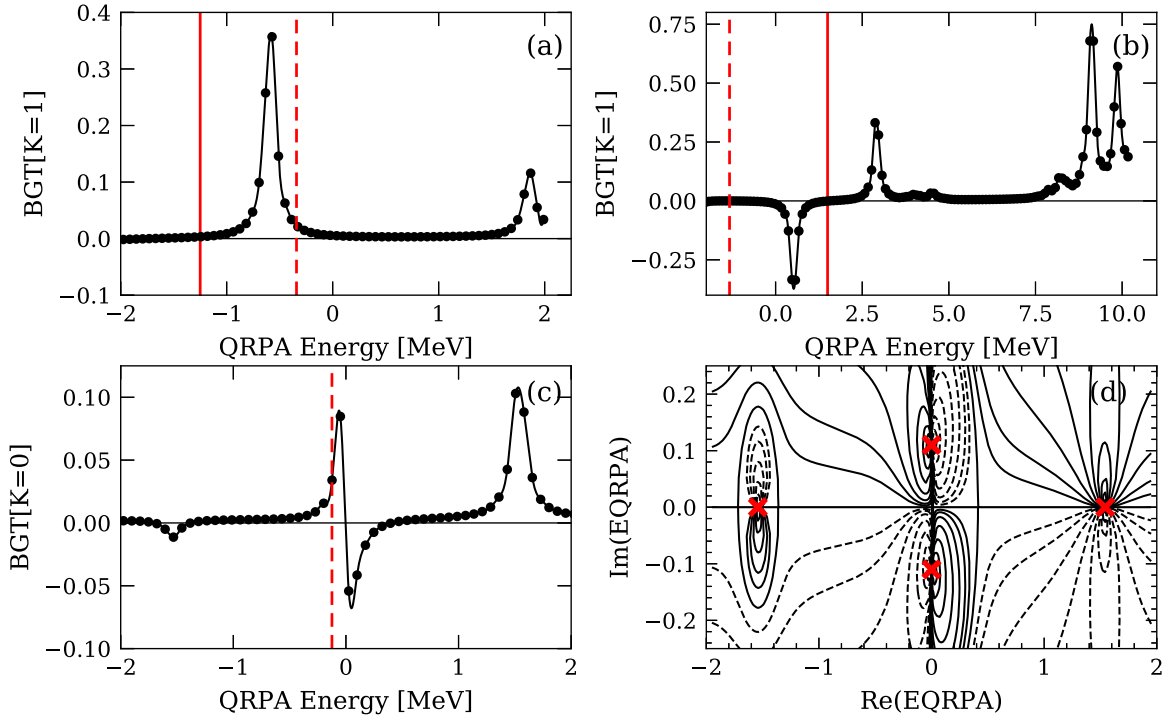

FIG. 3. Examples in which contour integration fails. The dashed vertical line indicates the left bound of the contour from Eq. (18), while the solid line indicates the adjusted bound required to correct the rate. (a) and (b) The Gamow-Teller (K=1) strength function for ^{63}Co and ^{53}Sc, respectively. (c) Illustration of an imaginary pole in the response function of ^{173}Er, and (d) the response in the full complex plane, indicating poles near $\omega = \pm 0.1i$.

half-lives shrink by more than an order of magnitude, when a low-lying β-minus transition is missing from the original contour. Some half-lives increase slightly after we remove positive contributions from imaginary poles. Orange triangles in Fig. 2(b) correspond to nuclei with negative total decay rates that became positive after correction.

Our random sample suggests that about 6% of our unexamined results should be corrected simply, by shifting the left bound of the contour, and about 15% may require more intricate corrections. Only a single half-life in the random sample changes by more than 5%, however (it changes by 30%). Thus, the corrections to unverified half-lives are very likely small compared to the average error in our rates (see Fig. 6). Nuclei with half-lives that require significant correction very probably belong to the suspicious set that we have just analyzed.

Finally, we should mention that numerical error is an additional source of small negative contributions to rates. Both the HFB and FAM solutions contain numerical error from several sources, e.g., incomplete convergence, truncation, etc. These errors are compounded in the final strength function and amplified by the phase space. If a rate is very small, the contour integral that generates it can suffer from incomplete cancelation of large oscillations. In compiling our final table of half-lives, presented here as Supplemental Material [43], we break each rate into contributions from each multipole, set any negative contributions to zero, and re-sum. This procedure usually changes rates by less than 5%.

In Fig. 4 we compare our final results with 2019 ENSDF experimental data [5] for nuclei with experimental half-lives less than 10^6 s. We highlight half-lives that are corrected, as in Fig. 2(b), and find that corrections almost always improve the agreement with experiment. The majority of our data fall within one or two orders of magnitude of experiment for half-lives less than 1000 s. In the next section, we will quantify more rigorously the theoretical uncertainties associated with such calculations.

Figure 5 displays the contributions to decay rates of first-forbidden operators. We find, as do other groups, that first-forbidden contributions are important in many nuclei and

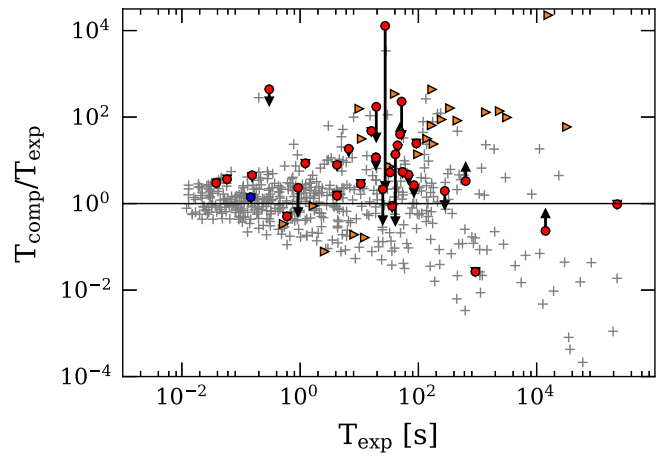

FIG. 4. Same as Fig. 2(b) but compared with 2019 ENSDF half-life data and vs experimental half-life. Only odd nuclei are shown.

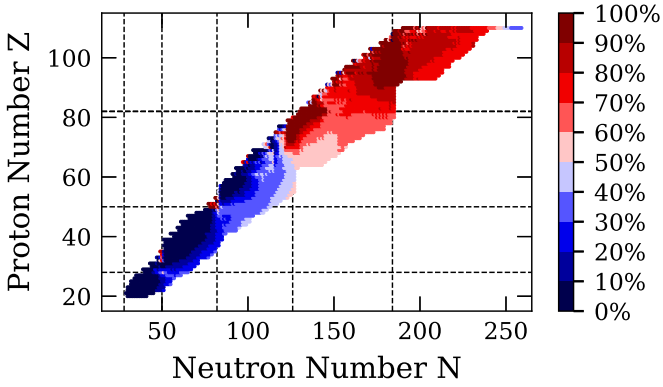

FIG. 5. First-forbidden contribution to the rates. Dashed lines indicate the magic numbers 28, 50, and 82 for protons, and 28, 50, 82, 126, and 184 for neutrons.

observe competing effects: Forbidden contributions scale with the nuclear radius and Q value, becoming important in heavier nuclei far from stability, but they also become important near stability and closed shells where the allowed rate is very small and allowed contributions are suppressed.

B. Error analysis

One major challenge facing large-scale calculations is the quantification of uncertainty. Most of the nuclei considered here are not experimentally accessible, and so we lack an experimental benchmark with which to evaluate our calculations. A simple way to deal with this challenge is to develop a *model* for the error. The model can be fit to data where available, and then extrapolated or interpolated to estimate errors for the remaining data. We use the simple model developed in Ref. [21], which we summarize here. The error parameter of interest is, for the i^{th} nucleus [11],

$$r_i = \log_{10}\left(\frac{t_{\text{th}}}{t_{\text{exp}}}\right). \tag{20}$$

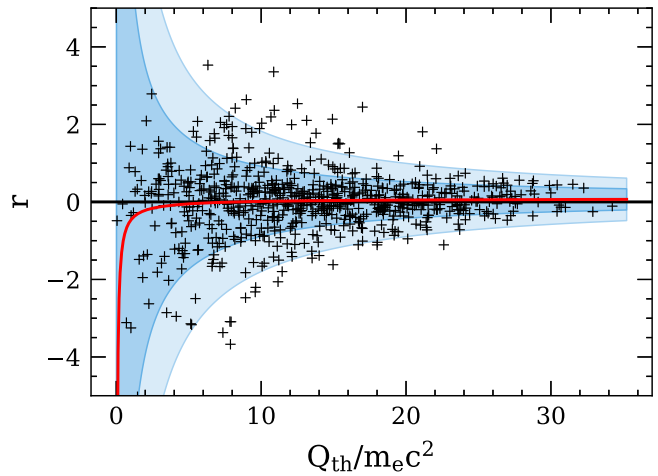

FIG. 6. Bayesian fit to the bias function and one- and two-standard-deviation bands.

To motivate a regression model for this parameter, we assume that there is a single dominant transition to a state near the daughter ground state, and that the forbidden shape factors depend much less on the Q value than does the allowed phase space. These assumptions allow us to assign a single effective Q value and shape factor C_{eff} to the decay; cf. [32] for the definition of the shape factor C. Using q_{eff} to denote the effective Q value in units of electron mass ($q_{\text{eff}} = Q_{\text{eff}}/m_ec^2$), we model the error r_i on the rate, as a function of the theoretical Q value and charge of the daughter nucleus, as

$$r_i\left(q^{\text{th}}_{\text{g.s.}}, Z_f\right) \approx c_{r_i} + f_r\left(q^{\text{th}}_{\text{g.s.}} + 1, Z_f\right) q_{r_i}, \tag{21}$$

where the errors in the effective shape factor c_r, and the effective Q value q_r are defined by

$$c_r \equiv \log_{10}\frac{C^{\text{exp}}_{\text{eff}}}{C^{\text{th}}_{\text{eff}}}, \quad q_r \equiv \frac{q^{\text{exp}}_{\text{eff}} - q^{\text{th}}_{\text{eff}}}{\ln 10}, \tag{22}$$

and the Q-value dependence is carried by the phase space factor,

$$f_r(q+1, Z_f) \equiv \frac{1}{f(q+1, Z_f)}\frac{df(q+1, Z_f)}{dq}. \tag{23}$$

Next, we assume that the c_{r_i} and q_{r_i}, which depend on the nucleus i, are each normally distributed random variables with widths that are independent of the Q value, and that the distributions for c_{r_i} and q_{r_i} contain a systematic bias that is independent of the nucleus and the Q value. These assumptions allow us to write the error parameters for nucleus i in the form,

$$\begin{aligned} c_{r_i} &= b_c + \epsilon_c, \quad \epsilon_c \sim \mathcal{N}(0, \sigma_c), \\ q_{r_i} &= b_q + \epsilon_q, \quad \epsilon_c \sim \mathcal{N}(0, \sigma_q), \end{aligned} \tag{24}$$

where b_c, b_q, σ_c, σ_q are still undetermined parameters. Finally, because the assumptions of the model are best for large Q values, we can make use of the Primakoff-Rosen approximation to the allowed phase space [44], which lets us express $f_r(q+1, Z_f)$ as a simple rational function with no explicit dependence on the charge Z_f of the daughter nucleus:

$$\begin{aligned} f_r(q+1, Z_f) &\approx f^P_r(q) \\ &\equiv \frac{5(q+1)^4 - 20(q+1) + 15}{(q+1)^5 - 10(q+1)^2 + 15(q+1) - 6}. \end{aligned} \tag{25}$$

We then end up with a one-dimensional, nonlinear error model with noise:

$$r_i\left(q^{\text{th}}_{\text{g.s.}}\right) = b_c + f^P_r\left(q^{\text{th}}_{\text{g.s.}}\right) b_q + \epsilon_i, \quad \epsilon_i \sim \mathcal{N}(0, \sigma_r). \tag{26}$$

Because c_r and q_r are independent, their widths add in quadrature. We find, however, that only σ_q is important and therefore take the width of the total noise term to be

$$\sigma_r\left(q^{\text{th}}_{\text{g.s.}}\right) = \sqrt{\sigma_c^2 + \left(f^P_r\left(q^{\text{th}}_{\text{g.s.}}\right)\sigma_q\right)^2} \approx f^P_r\left(q^{\text{th}}_{\text{g.s.}}\right)\sigma_q. \tag{27}$$

That leaves three unknown parameters b_c, b_q, σ_q to be determined.

To estimate the parameters, we use our own python adaptation of a Metropolis Monte Carlo code from Ref. [45] to

sample the un-normalized Bayesian posterior distributions of $\beta = \tan^{-1} b$ and σ_q, with priors,

$$P(\beta_c) = P(\beta_q) = \frac{1}{2\pi}, \quad P(\sigma_q) \propto \log(\sigma_q). \tag{28}$$

The sampling probability distribution is a multivariate Gaussian with a variance of $(0.02)^2$ for all three parameters. Following a burn-in period of 200 000 steps, we retain every 100^{th} iteration from the next million steps to reduce autocorrelation. From Gaussian kernel density estimates of the resulting distributions we estimate the most likely values, for $Q > 2$ MeV, to be $b_c = 0.088$, $b_q = -0.163$, and $\sigma_q = 1.984$. Figure 6 shows the resulting confidence regions on top of our entire data set. We find hardly any bias, indicating that our half-lives are equally likely to be over- and underpredicted. The model is not reliable for very small Q values, but for moderate to large Q values it predicts that the majority of our calculated half-lives will differ from experiment by less than one order of magnitude. The data is slightly non-Gaussian, with the one and two standard deviation bands capturing 76% and 94% of the 718 data points, respectively.

One may wonder whether the discrepancies between our computed rates and the experimental rates are due primarily to errors in the HFB Q values or to errors in the FAM strength distributions. The two are entangled in the expression for the rate, and so the question is not easy to answer in general. When the Q value is very small, however, the few daughter states that contribute to the decay have an energy that is very close to that of the endpoint. The fifth power of the difference between these two energies enters the decay rate, and so a slight error in the Q value has a large effect on the rate. When Q is larger, many states contribute to the rate and their energies are far from the endpoint, so that errors in the Q value have less of an effect on the rate than errors in excitation energies or strengths.

C. Comparisons

To evaluate our data where experimental values are unavailable, we compare our results to those of other global β-decay calculations. The authors of Ref. [17] (labeled "Homma" in Fig. 7) conducted a microscopic pnQRPA calculation with schematic allowed and unique first-forbidden interactions, and treated odd nuclei perturbatively. Reference [10] (labeled "Nakata") carried out a macroscopic calculation within the semigross theory. Reference [11] (labeled Möller) combined microscopic and macroscopic approaches, using the finite-range droplet model for ground-state properties, the pnQRPA with an empirical spreading for Gamow-Teller strength, and the gross theory for first-forbidden contributions. More recently, Ref. [46] (labeled "Costiris") applied a neural network to predict half-lives. Finally, Ref. [12] (labeled "Marketin") conducted a fully self-consistent covariant pnQRPA calculation with local fits to the isoscalar pairing strength, treating odd nuclei as if they were fully paired even nuclei with an odd number of nucleons on average.

To compare our results to those of the other papers, we use the quality measures outlined, e.g., in Ref. [11]: the mean (M_r)

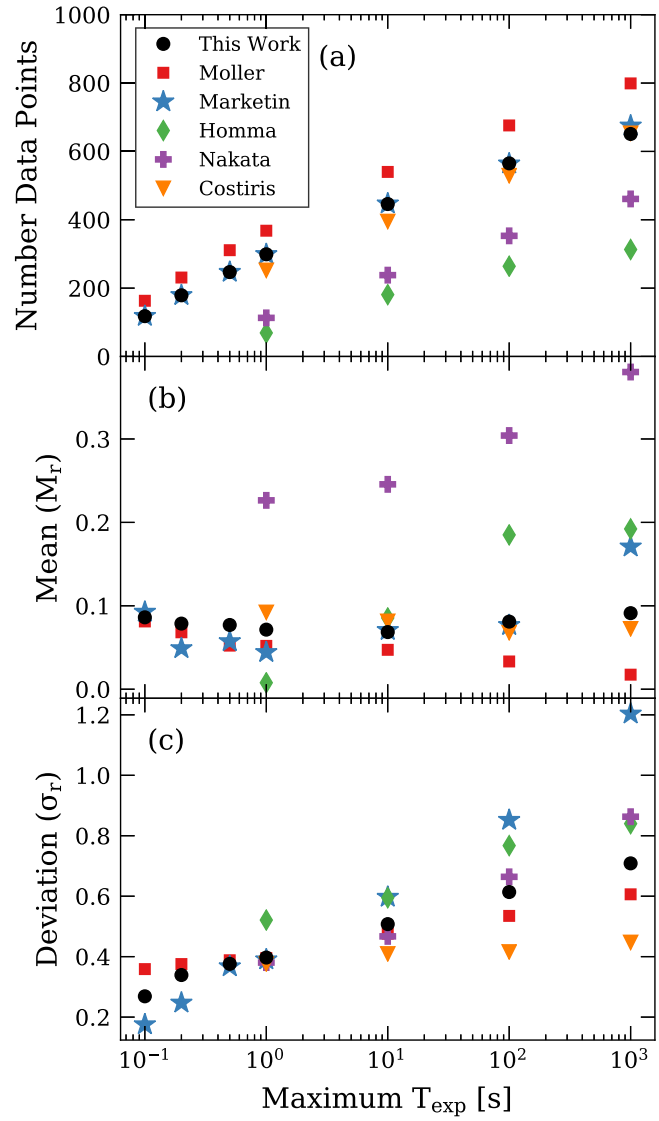

FIG. 7. Comparison of error-evaluation parameters among results of Refs. [12] (Marketin), [11] (Möller), [46] (Costiris), [10] (Nakata), and [17] (Homma).

and standard deviation (σ_r) of the error parameter in Eq. (20),

$$M_r = \frac{1}{n}\sum_{i=1}^{n} r_i, \quad \sigma_r = \left[\frac{1}{n}\sum_{i=1}^{n}(r_i - M_r)^2\right]^{1/2}. \tag{29}$$

We present these measures for the set of nuclei with experimental half-lives less than 1000 s, 100 s, 1 s, 0.5 s, 0.2 s, and 0.1 s. For Refs. [10,17,46] we take the measures directly from the corresponding paper. References [11,12] supplied their data set as Supplemental Material, and we recompute the quality measures with the more recent 2019 ENSDF experimental half-lives [5]. Figure 7 summarizes the results. The differences in experimental data sets considered in each paper can be seen in part by noting the number of data points used to compute the quality measures. The errors for Ref. [12] are somewhat larger for long-lived isotopes than the values given in that paper because we include all the calculations in odd

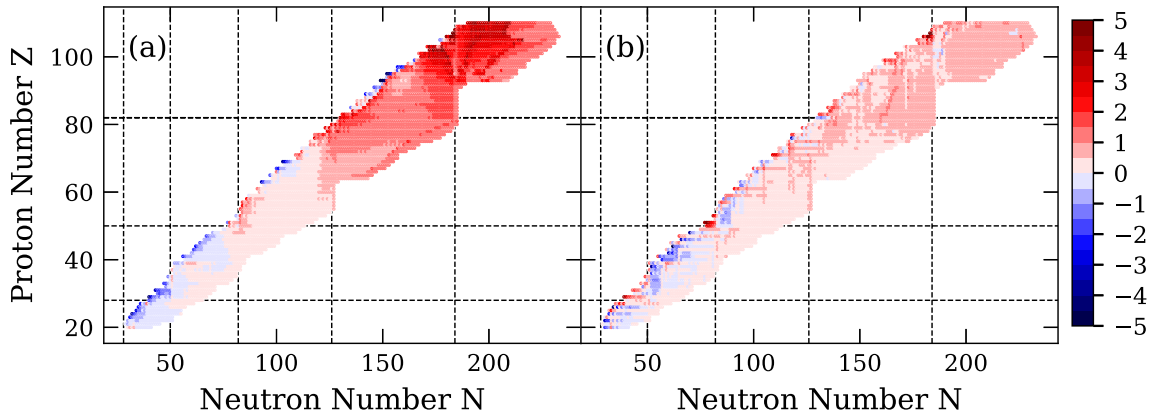

FIG. 8. Base-10 logarithm of the ratio of our half-lives to those of (a) Ref. [12] and (b) Ref. [11]. Dashed lines indicate the same magic numbers as in Fig. 5.

nuclei, while the authors excluded a few that they considered outliers. In general, our calculation is comparable in fidelity to the others. Unlike those, however, its treatment of odd nuclei is fully self-consistent, capturing in part the one-quasiparticle nature of such states through the EFA, and it uses a single energy functional with no local adjustments. Figure 8 compares all our results with those provided in Refs. [11,12]. We generally predict longer half-lives than the other two models in heavier nuclei, and slightly shorter half-lives in lighter nuclei. The vast majority of our numbers fall within one order of magnitude of those of Ref. [11]. Both we and Ref. [11] predict significantly longer half-lives in heavy isotopes than does Ref. [12]. There do not appear to be any other significant systematic differences among the results.

V. CONCLUSIONS

Using the statistical extension of the charge-changing finite-amplitude method, we computed β-decay half-lives of almost all odd-mass and odd-odd nuclei on the neutron-rich side of stability, in a fully microscopic and self-consistent way. The equal filling approximation allows us to retain time-reversal symmetry while still largely including the effects of core polarization by the odd nucleon. We showed that in a few cases the EFA leads to the appearance of negative and even imaginary eigenvalues. Overall our half-lives are similar to those of other global calculations in reproducing experimental data. We supplemented these calculations with an estimate of theoretical uncertainties, which suggest that calculated half-lives fall within two orders of magnitude of experimental values for nuclei with Q values greater than about 2 MeV. We also find, as do other groups, that first-forbidden contributions are important in many nuclei. We provided all the half-lives described here, along with associated ground-state properties, error estimates, and Gamow-Teller strength distributions, in the Supplemental Material [43].

We plan to extend our methods in several ways:

(1) We will use the statistical FAM with the grand canonical ensemble for finite temperature β-decay calculations. Decay at nonzero temperature plays an important role in neutron-star mergers and core-collapse supernovae [47,48].
(2) We will improve the ability of the FAM to capture low-energy strength by including correlations beyond the QRPA. Although one must be careful in combining such correlations with density functionals, several procedures exist for doing so [49–51]. An efficient implementation of an extension to the FAM would allow better global calculations.
(3) Finally, we will better treat the weak interaction. Here we restrict ourselves to the impulse approximation, neglecting many-body currents completely. Recent work shows that such currents account for a significant fraction of the quenching of Gamow-Teller strength [52]. With an additional extension of the pnFAM we can take two-body currents into account.

Our calculations are also an important milestone in the development of a consistent description of the fission process within nuclear DFT [53]. Although spontaneous fission-fragment half-lives, fragment distributions, and fragment excitation energies can already be computed in DFT, our work paves the way for a description of the deexcitation of the fragments, including γ emission and β decay, within the same framework.

ACKNOWLEDGMENTS

Many thanks to M. Mustonen and T. Shafer for guidance on the pnFAM, and to S. Guilliani for helpful discussions on β decay. This work was supported in part by the Nuclear Computational Low Energy Initiative (NUCLEI) SciDAC-4 project under US Department of Energy Grants No. DE-SC0018223 and No. DE-SC0018083, and by the Department of Energy under Grant No. DE-SC0013365 and the FIRE collaboration. Some of the work was performed under the auspices of the US Department of Energy by Lawrence Livermore National Laboratory under Contract No. DE-AC52-07NA27344. Computing support came from the Lawrence Livermore National Laboratory (LLNL) Institutional Computing Grand Challenge program.

[1] E. M. Burbidge, G. R. Burbidge, W. A. Fowler, and F. Hoyle, Rev. Mod. Phys. **29**, 547 (1957).
[2] B. S. Meyer, Annu. Rev. Astron. Astrophys. **32**, 153 (1994).
[3] B. P. Abbott *et al.* (LIGO Scientific Collaboration and Virgo Collaboration), Phys. Rev. Lett. **119**, 161101 (2017).
[4] C. J. Horowitz, A. Arcones, B. Cote, I. Dillmann, W. Nazarewicz, I. Roederer, H. Schatz, A. Aprahamian, D. Atanasov, A. Bauswein, T. C. Beers, J. Bliss, M. Brodeur, J. Clark, A. Frebel, F. Foucart, C. Hansen, O. Just, A. Kankainen, G. McLaughlin, J. Kelly, S. Liddick, D. Lee, J. Lippuner, D. Martin, J. Mendoza-Temis, B. T. Metzger, M. Mumpower, G. Perdikakis, J. Pereira, B. O'Shea, R. Reifarth, A. Rogers, D. Siegel, A. Spyrou, R. Surman, X.-D. Tang, T. Uesaka, and M. Wang, J. Phys. G: Nucl. Part. Phys. **46**, 8 (2019).
[5] Evaluated Nuclear Structure Data File (ENSDF) (2019), http://www.nndc.bnl.gov/ensarchivals.
[6] P. Möller, J. Nix, and K.-L. Kratz, At. Data Nucl. Data Tables **66**, 131 (1997).
[7] J. Engel, M. Bender, J. Dobaczewski, W. Nazarewicz, and R. Surman, Phys. Rev. C **60**, 014302 (1999).
[8] M. Mumpower, J. Cass, G. Passucci, R. Surman, and A. Aprahamian, AIP Adv. **4**, 041009 (2014).
[9] T. Shafer, J. Engel, C. Frohlich, G. C. McLaughlin, M. Mumpower, and R. Surman, Phys. Rev. C **94**, 055802 (2016).
[10] H. Nakata, T. Tachibana, and M. Yamada, Nucl. Phys. A **625**, 521 (1997).
[11] P. Möller, B. Pfeiffer, and K.-L. Kratz, Phys. Rev. C **67**, 055802 (2003).
[12] T. Marketin, L. Huther, and G. Martínez-Pinedo, Phys. Rev. C **93**, 025805 (2016).
[13] P. Ring and P. Schuck, *The Nuclear Many-Body Problem* (Springer, Berlin, Heidelberg, 2004).
[14] N. Schunck, *Energy Density Functional Methods for Atomic Nuclei* (IOP Publishing, Bristol, 2019).
[15] G. Bertsch, J. Dobaczewski, W. Nazarewicz, and J. Pei, Phys. Rev. A **79**, 043602 (2009).
[16] N. Schunck, J. Dobaczewski, J. McDonnell, J. Moré, W. Nazarewicz, J. Sarich, and M. V. Stoitsov, Phys. Rev. C **81**, 024316 (2010).
[17] H. Homma, E. Bender, M. Hirsch, K. Muto, H. V. Klapdor-Kleingrothaus, and T. Oda, Phys. Rev. C **54**, 2972 (1996).
[18] S. Perez-Martin and L. M. Robledo, Phys. Rev. C **78**, 014304 (2008).
[19] T. Duguet, P. Bonche, P.-H. Heenen, and J. Meyer, Phys. Rev. C **65**, 014311 (2001).
[20] G. F. Bertsch, C. A. Bertulani, W. Nazarewicz, N. Schunck, and M. V. Stoitsov, Phys. Rev. C **79**, 034306 (2009).
[21] M. T. Mustonen and J. Engel, Phys. Rev. C **93**, 014304 (2016).
[22] T. Nakatsukasa, T. Inakura, and K. Yabana, Phys. Rev. C **76**, 024318 (2007).
[23] P. Avogadro and T. Nakatsukasa, Phys. Rev. C **84**, 014314 (2011).
[24] T. Nikšić, N. Kralj, T. Tutiš, D. Vretenar, and P. Ring, Phys. Rev. C **88**, 044327 (2013).
[25] H. Liang, T. Nakatsukasa, Z. Niu, and J. Meng, Phys. Rev. C **87**, 054310 (2013).
[26] H. Liang, T. Nakatsukasa, Z. Niu, and J. Meng, Phys. Scr. **89**, 054018 (2014).
[27] T. Inakura, T. Nakatsukasa, and K. Yabana, Phys. Rev. C **80**, 044301 (2009).
[28] T. Inakura, T. Nakatsukasa, and K. Yabana, Eur. Phys. J. A **42**, 591 (2009).
[29] T. Inakura, T. Nakatsukasa, and K. Yabana, Mod. Phys. Lett. A **25**, 1931 (2010).
[30] M. Stoitsov, M. Kortelainen, T. Nakatsukasa, C. Losa, and W. Nazarewicz, Phys. Rev. C **84**, 041305(R) (2011).
[31] T. Oishi, M. Kortelainen, and N. Hinohara, Phys. Rev. C **93**, 034329 (2016).
[32] M. T. Mustonen, T. Shafer, Z. Zenginerler, and J. Engel, Phys. Rev. C **90**, 024308 (2014).
[33] T. Nakatsukasa, J. Phys.: Conf. Ser. **533**, 012054 (2014).
[34] N. Hinohara, Phys. Rev. C **92**, 034321 (2015).
[35] N. Hinohara, M. Kortelainen, and W. Nazarewicz, Phys. Rev. C **87**, 064309 (2013).
[36] N. Hinohara, M. Kortelainen, W. Nazarewicz, and E. Olsen, Phys. Rev. C **91**, 044323 (2015).
[37] H. M. Sommermann, Ann. Phys. (NY) **151**, 163 (1983).
[38] A. L. Goodman, Nucl. Phys. A **352**, 30 (1981).
[39] A. Bohr and B. R. Mottelson, *Nuclear Structure Volume II: Nuclear Deformations* (World Scientific, Singapore, 1998).
[40] P. G. Reinhard, D. J. Dean, W. Nazarewicz, J. Dobaczewski, J. A. Maruhn, and M. R. Strayer, Phys. Rev. C **60**, 014316 (1999).
[41] R. N. Perez, N. Schunck, R. D. Lasseri, C. Zhang, and J. Sarich, Comput. Phys. Commun. **220**, 363 (2017).
[42] L. N. Trefethen, *Approximation Theory and Approximation Practice* (Society for Industrial and Applied Mathematics, 2020).
[43] See Supplemental Material at http://link.aps.org/supplemental/10.1103/PhysRevC.102.034326 for tables of β-decay properties and strength functions.
[44] J. Suhonen, *From Nucleons to Nucleus: Concepts of Microscopic Nuclear Theory* (Springer, Berlin, Heidelberg, 2007).
[45] C. A. L. Bailer-Jones, *Practical Bayesian Inference: A Primer for Physical Scientists* (Cambridge University Press, Cambridge, 2017).
[46] N. J. Costiris, E. Mavrommatis, K. A. Gernoth, and J. W. Clark, Phys. Rev. C **80**, 044332 (2009).
[47] K. Langanke and G. Martínez-Pinedo, Nucl. Phys. A **673**, 481 (2000).
[48] K. Langanke, E. Kolbe, and D. J. Dean, Phys. Rev. C **63**, 032801(R) (2001).
[49] D. Gambacurta, M. Grasso, and J. Engel, Phys. Rev. C **92**, 034303 (2015).
[50] C. Robin and E. Litvinova, Eur. Phys. J. A **52**, 205 (2016).
[51] Y. F. Niu, Z. M. Niu, G. Colò, and E. Vigezzi, Phys. Lett. B **780**, 325 (2018).
[52] P. Gysbers, G. Hagen, J. D. Holt, G. R. Jansen, T. D. Morris, P. Navrátil, T. Papenbrock, S. Quaglioni, A. Schwenk, S. R. Stroberg, and K. A. Wendt, Nat. Phys. **15**, 428 (2019).
[53] N. Schunck and L. M. Robledo, Rep. Prog. Phys. **79**, 116301 (2016).